Applied Energy 247 (2019) 155–170

Contents lists available at ScienceDirect

Applied Energy

journal homepage: www.elsevier.com/locate/apenergy

Adaptive measures for mitigating urban heat islands: The potential of thermochromic materials to control roofing energy balance

C. Fabiani[a], A.L. Pisello[a,b,*], E. Bou-Zeid[c], J. Yang[c], F. Cotana[a,b]

[a] CIRIAF – Interuniversity Research Center, University of Perugia. Via G. Duranti 67, 06125 Perugia, Italy
[b] Department of Engineering University of Perugia, Via G. Duranti 97, 06125 Perugia, Italy
[c] Department of Civil and Environmental Engineering, Princeton University, 59 Olden Street, 08540 NJ, USA

HIGHLIGHTS

- Thermochromic roof coating is developed and experimentally tested.
- The thermochromic solution is implemented in an urban canopy model.
- The thermochromic solution effect is assessed in terms of urban heat island mitigation potential.
- Benchmarking against more common roofing solutions is carried out.
- The effect of different transition temperatures is evaluated.

ARTICLE INFO

Keywords:
Urban canopy model
Urban canyon
Urban heat island
Energy efficiency
Building envelope
Albedo
Thermochromic materials

ABSTRACT

In recent years, the urgent need for reducing building energy consumption has prompted the scientific community to investigate and develop new adaptive materials for the built environment, and to use field monitoring and multiscale advanced modeling for analyzing and improving the urban microclimate conditions using these new materials. In this work, the Princeton Urban Canopy Model (PUCM) is used to investigate the potential of an advanced urban roofing material to counteract urban overheating in summer, while simultaneously taking advantage of solar passive heating in winter. The roofing applications are characterized by an adaptive dynamic temperature-dependent optical behavior. In particular, the effect of thermochromic materials on local energy transport phenomena is assessed and benchmarked against a traditional dark roof and a more common cool roof solution. These materials undergo a rapid albedo increase when the surface temperature exceeds a certain threshold. Results demonstrate that using thermochromic materials produces a smart optical response to local environmental stimuli and allows enhanced shortwave solar reflection in summer conditions, reduced reflected solar fraction in winter, and adaptive properties during transition periods.

1. Introduction

In the last decades, extensive urban expansion and population growth have exacerbated several environmental problems such as resource depletion, air pollution and local climate change [1]. Among these phenomena, the best documented one is the so called urban heat island (UHI), which consists of a local temperature increment affecting metropolitan areas with respect to their rural surroundings [2] and where the maximum temperatures are generally experienced within the densest city blocks [3].

This phenomenon can significantly affect the local microclimate, producing persistent high temperatures. As a result, it can be a threat to the livability of a city and can have detrimental ecological and environmental impacts including biodiversity loss [4] and increased water consumption [5]. As a matter of fact, excessive air temperatures can drastically reduce the effectiveness of natural and nighttime ventilation, and may also be strongly correlated with elevated ozone and nitrogen oxides concentration levels [6]. Consequently, it is now widely recognized that the UHI negatively affects human comfort level during hot periods, contributing to human diseases and health risks particularly among the very young and the elderly [7,8].

Further exacerbating the risk is recent evidence that UHIs interact synergistically with regional heat waves [9], producing repercussions that might exceed a simple superposition of the two hazards [10].

* Corresponding author.
E-mail address: anna.pisello@unipg.it (A.L. Pisello).

https://doi.org/10.1016/j.apenergy.2019.04.020
Received 6 August 2018; Received in revised form 4 April 2019; Accepted 9 April 2019

Beyond their health and environmental impacts, heat islands also have important implications on buildings energy consumption since increased air temperatures exacerbate building cooling loads [11] and increase peak electricity demand [12]. According to Kikegawa et al., this phenomenon could be particularly detrimental to the low-latitude cities of Asia and Africa, which are expected to experience a rapid population increase in the near future and mostly concentrate their energy demand in the cooling season [13]. Additionally, although urban heat islands are generally associated with large metropolitan areas, recent research contributions suggest that even relatively small cities, i.e. of just over 200,000 people, could be affected by this detrimental phenomenon, which consequently could be more common than expected [14].

All this considered, a deeper understanding of the main causes and effects of the UHI is nowadays of paramount importance. Perhaps of even more importance however is the development of efficient mitigation strategies and solutions. As a result, in recent years, several research contributions have been focusing on the effect of specific strategies such as shading of buildings, use of green and high albedo surfaces, and introduction of water bodies and air ventilation improvement on the magnitude of the local heat island in different cities worldwide [15]. In particular, using green and cool roofing materials was found to be highly effective in reducing both surface and air temperature peaks in the urban environment during summer [16].

Sohaili et al., for example, found a 4.3 °C surface temperature reduction during the hottest hour of the hottest summer day, together with a higher relative humidity when comparing an existing green roof and a classic dark roof solution [17]. Moghbel and Erfanian Salim, on the other hand, registered a 3.7 °C and an 8.46% reduction in terms of average air temperature and relative humidity when comparing the investigated green roof and a reference bitumen application [18]. On a yearly basis, Chun et al. showed that the introduction of greenery reduces temperatures in summer while increasing them in winter, thus demonstrating that greening and land-use policies for UHI mitigation should account for seasonal effects to achieve year-long effectiveness [19].

Beyond these results, numerous other research contributions demonstrated the beneficial effect of vegetated roofs and walls in buildings. However, these applications also require extensive efforts for their implementation from both an economic and a practice point of view [20]. On top of that, it is also widely acknowledged that green roofs mitigation effect is deeply connected to the amount of water in the substrate and in the greenery itself. Therefore, an irrigation system might be required for an effective green roof application [21]. Based on this, several research contribution have stressed the interaction between the potential water buffering capacity of a green infrastructure and its implications in terms of water depletion for sustainable urban planning. In particular, Yang et al. used the Weather Research and Forecasting (WRF) model within Phoenix metropolitan area, Arizona, United States, considering water-saving and fully-greening scenarios [22]. They found that modifications of the existing green infrastructure and irrigation practices can significantly influence the thermal environment of that desert environment.

All this considered, the attention of the scientific community was recently drawn to the implementation of innovative roof applications, characterized by optimized solar reflectance and thermal emittance capability, i.e. the so called cool roof solutions. As a matter of fact, these surface treatments are cost effective and easy to implement, and additionally, they require much less maintenance than classic green roofs. Several kinds of applications have been investigated using both simulations and experimental studies. These solutions are typically classified as: membranes, coatings, paintings, metal roofs, shingles, and tiles [23], and their effect in terms of surface and air temperature reduction is usually comparable to that of vegetated roofs [16].

The performance of roof paintings and coatings, for example, which are simply composed by transparent polymers and white pigments such as titanium dioxide, was extensively investigated by Synnefa et al., who monitored the effect of fourteen different paintings in terms of surface temperature, infrared emittance and surface reflectance [24]. They found a 4 °C and 2 °C reduction in summer conditions during the day and the night, respectively. By using advanced clay tiles, a 14 °C surface temperature difference was reached in a cool steep-slope roof compared to a conventional dark roof in the work by Mangiarotti et al. [25], while a surface temperature reduction between 5 and 14 °C and a heat flux reduction of 13–21% were detected by Levinson et al. after the application of NIR-reflective roof tile coatings [26].

Most recently, cool roofing membranes have been implemented with thermal storage effect as a passive technique for building thermal-energy efficiency and urban heat island mitigation. Pisello et al., for instance, developed an innovative polyurethane based membrane combining cool pigments and phase change materials (PCMs) that allows surface peak temperature buffering and improves durability due to reduced thermal stress within the polymer-based membrane [27,28]. However, because cool roofs reflect most of the incoming solar radiation, and re-emit most of the absorbed one in the long-wave range, cool materials were also found to reduce the solar gains through the building walls and roof in winter, and consequently, increase the building energy use for heating purposes [29]. This was found both at the single building, as demonstrated by Pisello et al. on their study about the indoor thermal comfort condition of a residential single family house located in central Italy [30], and at the inter-building scale, as shown by Yang et al., who recommended a city-by-city approach rather than a one-solution-fits-all strategy for the large scale deployment of reflective materials [31].

The adverse effect of high albedo solutions becomes even more severe during extreme cold waves where a few degrees can be crucial to health risks of residents, negating some of the positive impacts of UHIs during winter time and extreme cold weather [32]. Therefore, in recent years, the scientific community has been trying to develop advanced solutions, capable of reducing the potential winter downside of such applications. In particular, several researchers have investigated the possibility of using thermochromic materials, i.e. parcels that respond to the surrounding environment by reversibly changing their optical properties as a function of temperature [33–35].

According to Garshasbi and Santamouris, two different groups of thermochromic materials exist: (i) dye-based (mostly Leuco dyes), and (ii) non-dye-based thermochromic materials [36].The latter represent the avant-garde solution for this field of application, and can be further divided into (i) materials whose color change mechanism is associated to fascinating effects at the nano-scale (e.g. quantum dots, plasmonics and photonic crystals) [37], or (ii) composites whose unique properties originate from the molecular rearrangements due to temperature change (e.g. conjugated polymers, liquid crystals and Schiff bases) [38]. Although these materials represent the cutting edge of thermochromism, they are still very expensive and, as such, they have not been operationally used in the built environment [36].

Regarding the thermochromic functional dyes, they can also be divided into two classes, i.e. dye-polimer and leuco dyes composites. In dye-polymers, the driving force of the thermochromic effect is the interplay between the pH-indicator dye and the polymer matrix; therefore, the single components do not actually possess any thermochromic properties [39]. On the other hand, in leuco dyes composites, which consist of three components: color former (the leuco dye), color developer and co-solvent the material itself is capable of switching from the colorless (leuco) to the colored (zwitterionic) state through the temperature change [40]. This last kind of application has been used to produce different types of building components with the aim of investigating their optical, thermal and mechanical properties, but it was reported to undergo photo-degradation in outdoor applications [41]. Despite these hurdles, the result of these studies is the production of innovative building coatings capable of tuning their solar reflectivity as a function of the local temperature boundary conditions [42]. While

these materials were investigated for given sites using both climatic chambers and natural climatic conditions [43], how their impacts scale with application footprint remains unknown.

In recent years, high-resolution numerical simulations of UHI under real atmospheric conditions have been increasingly used to investigate the effect of various mitigation strategies, with the aim of providing a solid decision framework for policy makers worldwide [16,44]. At present, they provide the most suitable approaches to model and test large-scale deployments of mitigation measures. These kind of simulations are highly sensitive to the specific urban canopy model (UCM) used to represent the urban environment and the related surface energy budgets: the more realistic the model and the representation of the physics of the mitigation option are, the more reliable the results will be. For this reason, several researchers have been focusing on the development of advanced urban canopy models that represent the heat-transfer physics and hydrological processes involved in the surface energy budget faithfully [45–47].

In this work, an advanced leuco dye-based thermochromic coating is produced and experimentally tested by means of advanced thermo-optic analyses. Later on, the Princeton Urban Canopy Model (PUCM) is used to investigate the potential application of this coating as a UHI mitigation strategy, and explore the advantages of optimized thermochromic membranes over purely cool or dark roofs at the inter-building scale. Therefore, the results from the numerical analyses are critically examined with the aim of evaluating the expected benefits deriving from the introduction of the leuco dye-based solution in the built environment. This then can be used to guide the development of the aforementioned novel thermochromic solutions for urban applications.

The next section describes the development of the thermochromic membrane and its experimental characterization. Section 3 presents the modeling methodology and the validation procedure. Finally, Section 4 presents and discusses the results with bench-marking with respect to a traditional dark roof configuration and a more common cool roof application.

2. Development and testing of the thermochromic roof coating

2.1. Thermochromic coating production

In this work, microencapsulated leuco-based thermochromic pigments from Arcacolours S.R.L. with an average particle size of 5 μm were used to produce an advanced solvent-based coating for building applications. The pigments were black in their cold state and translucent in their warm state, with a transition temperature of about 20 °C. They were used to produce a finishing paint to be applied over a soiled polyurethane-based membrane to provide the existing cool roof solution with a dynamic optical behavior as a function of the local temperature boundary conditions. The paint consisted of 50 wt% a toluene–xylene based solvent; 30 wt% petroleum-derived resins; and 20 wt% thermochromic pigment. A double layer of thermochromic paint was sprayed over the polyurethane membrane, to ensure a more uniform result (see Fig. 1).

2.2. Thermo-optic characterization of the coating

Optical characterization of the produced thermochromic coating was performed by means of a solar spectrophotometer (SolidSpec-3700) equipped with a 60 mm-diameter integrating sphere with a wavelength accuracy of 0.1 nm. The tests were performed according to the international test method reported in ASTM E 903-96 [48] This ASTM standard describes the procedure to perform measurements of spectral near-normal hemispherical reflectance over the range of 300–2500 nm with a lab instrument. The solar reflectance values were defined by weighting the wavelength with respect to reference solar spectra (according to reference values [49]).

The advanced coating was characterized both in the colored and the non-colored phase, i.e. below and above the reference transition temperature of 20 °C. Fig. 2 reports results from the spectrophotometer analysis. As can be seen, the thermochromic coating is characterized by a significantly different optical response in the range 400–780 nm when the colored and the non-colored phase are compared. On the other hand, a relatively negligible effect of the thermochromic transition can be detected in the NIR region. Such results cause the average reflection coefficient of the membrane to switch between about 0.35 and 0.55, i.e. colored and non-colored phase, respectively.

3. Methodology

3.1. UCM description and setup

In this work, a state-of-the-art urban canopy model (PUCM) developed by Wang et al. at Princeton University [45], is extended to investigate the potential of thermochromic roof coating as an innovative UHI mitigation strategy. The Princeton urban canopy model considers the single-layer "big-canyon" representation for urban areas featuring a detailed surface exchange scheme that couples energy transport and hydrological processes over natural and engineered surfaces, also taking into account sub-facet heterogeneity. The model was validated under different climate conditions, using extensive field measurements taken in different towns and cities including Baltimore, Beijing, Phoenix, Vancouver, Princeton, and Montréal, in an offline (stand-alone) mode driven by 5 to 30-min averaged meteorological data obtained from meteorological towers [45,46,50,51]. In this paper, we will use this same validated offline mode where the urban feedbacks to the atmosphere are shut off, and atmospheric state observations are imposed on the UCM.

In the PUCM, the one-dimensional energy balance for an infinitesimally-thin interfacial layer of each considered i-th surface (i = ground, wall and roof), at the surface-air interface, is defined as:

$$R_n = H + LE + G \tag{1}$$

where R_n is the net radiation (defined as the sum of the net shortwave and longwave components); H is the sensible heat flux; LE is the latent heat flux (from soil evapotranspiration and/or plant transpiration); and G is the heat storage term (flux into the surface). The canyon air is treated as a separate thermal mass and any anthropogenic emissions would be directly released into that mass (except the emissions due to space heating that are indirectly represented by maintaining a fixed indoor temperature in the winter). Additionally, since the PUCM implements an explicit resolution for sub-facet heterogeneity in building walls, rooftops and ground facet, the thermo-optical properties of every single surface may be subdivided into individual subfacets. The specific properties of ground surfaces and building walls and roofs used in this work are based on the work by Ryu et al. [52], which also allows to take into account the effect of trees in the simulated canyon. The most important properties about the roof modeled in the UCM are shown in Table 1.

The albedo of the thermochromic roof is defined in order to dynamically change as a function of the roof temperature according to:

$$\alpha(T) = \alpha_{dark} + \frac{\alpha_{cool} - \alpha_{dark}}{2}(1 + erf(t_{norm})) \tag{2}$$

where $\alpha(T)$ is the albedo at temperature T; α_{dark} is the albedo for temperatures below the thermochromic transition temperature (TT); α_{cool} is the albedo for temperatures above the thermochromic transition temperature (TT); $erf(t_{norm})$ is the error function; and t_{norm} is the normalized time, defined as:

$$t_{norm} = count(t)\frac{2\pi}{t_{TT}} \tag{3}$$

where t_{TT} is the length of the thermochromic transition time interval, which was set to 1200 s [43], and count(t) is a counting function that

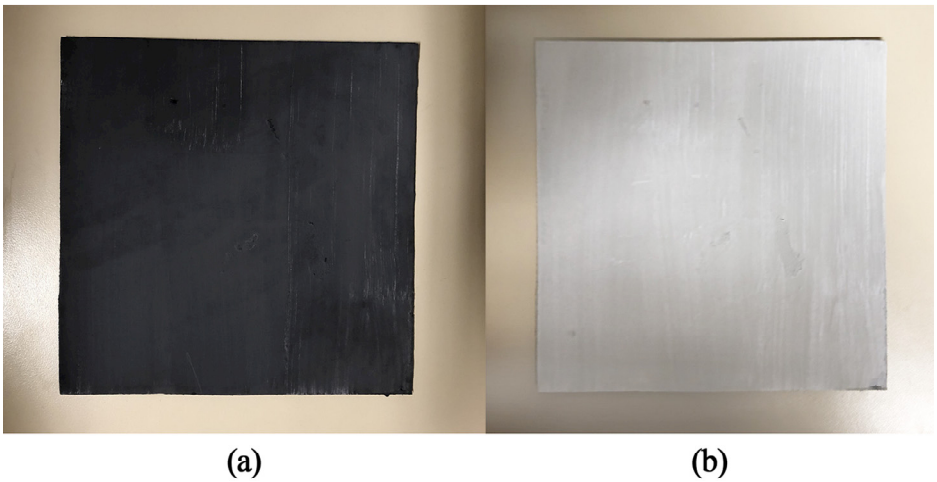

Fig. 1. Thermochromic roof coating in the (a) colored and in the (b) non-colored phase.

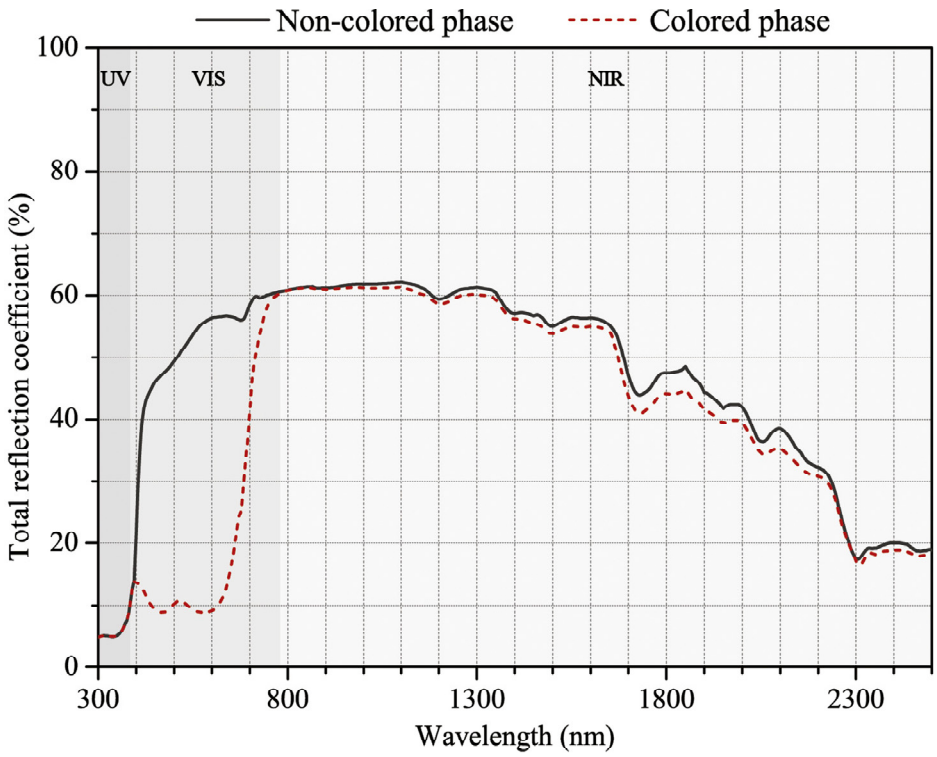

Fig. 2. Comparison between the optical response of the thermochromic roof coating in the colored and non-colored phase.

Table 1
Roof input parameters used in the urban canopy model (based on the work by Ryu et al. [52]).

Geometrical and thermo-optic parameters	Symbol	Value	Unit
Roof thickness	d_R	0.3	[m]
Cool roof surface albedo	α_{cool}	0.55	
Dark roof surface albedo	α_{dark}	0.15	
Roof surface emissivity	ϵ_R	0.95	
Roof thermal conductivity	k_R	0.94	[W m^{-1} K^{-1}]
Roof heat capacity	c_R	1.4	[MJ m^{-3} K^{-1}]

tracks the time elapsed from the beginning of a given thermochromic transition, defined as:

$$count(t) = \begin{cases} t_{TT} & \text{if } T(t-1) < TT \ \& \ count(t-1) > t_{TT} \\ count(t-1) - dt & \text{if } T(t-1) < TT \ \& \ count(t-1) \leqslant t_{TT} \\ 0 & \text{if } T(t-1) \geqslant TT \ \& \ count(t-1) < t_{T0} \\ count(t-1) + dt & \text{if } T(t-1) \geqslant TT \ \& \ count(t-1) \geqslant t_{T0} \end{cases} \quad (4)$$

where t_{T0} is equal to 0, and dt is the time interval of the simulation, i.e. 10 s. Fig. 3 shows the resulting trend for the count(t) function in response to a specific temperature profile.

3.2. Validation of the model

As previously explained in Section 1, thermochromic coatings represent an avant-garde application for the building sector, and their

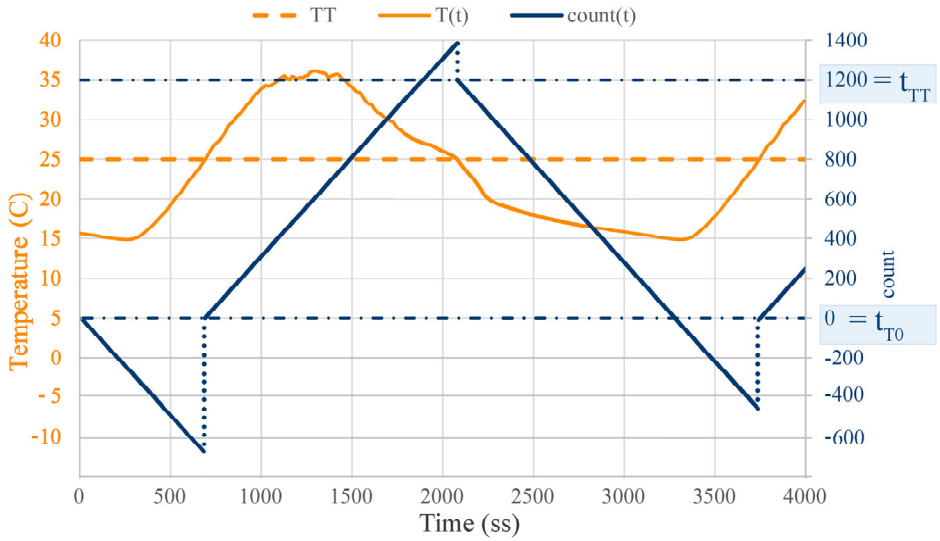

Fig. 3. Example of the count(t) function trend in response to a temperature profile for a surface with TT = 25 °C.

implementation at the inter-building scale has never been investigated so far. However, small samples of these dynamic coatings have been previously tested using real atmospheric forcings or in simulated environments within advanced climatic chambers [43].

In this work, we produced a reference stratigraphy having the same effective thermal properties of the roof simulated in the PUCM model and we used it to validate the thermal response of the dynamic material. The stratigraphy, characterized by a planar dimension of 0.20 × 0.20 m, was specifically designed in order to be integrated as the upper surface of a cubic box, made of 0.1 m thick extruded polystyrene (XPS) layers and 0.015 m thick vacuum insulation panels (VIP) (see Fig. 4a). It was produced using three different components, i.e. a 0.015 m thick water-proof roof membrane with a thermochromic coating, a 0.035 m thick extruded polystyrene (EPS) layer and a 0.050 m thick concrete slab, for a total thickness of about 0.1 m (see Fig. 4a). These specific materials and geometric dimensions were carefully selected in order to: (i) obtain similar periodic thermal transmittance (calculated according to the EN ISO 13786 standard [53]) between the equivalent experimental stratigraphy and the modeled one, (ii) guarantee a minimum air volume inside the box which was used to simulate the indoor environment of the building, (iii) allow the VIP-XPS box to be introduced within the controlled environment of a climatic chamber, and (iv) maintain at least an order of magnitude difference between the periodic thermal transmittance of the equivalent roof stratigraphy and the one of the insulation box (see Table 2). This last condition allowed us to consider the heat flux through the roof to be one-dimensional during the short duration of the validation tests.

The previously described experimental setup was housed within the test compartment of a climatic chamber model ATT DM340SR and exposed to a controlled environmental cycle reproducing the

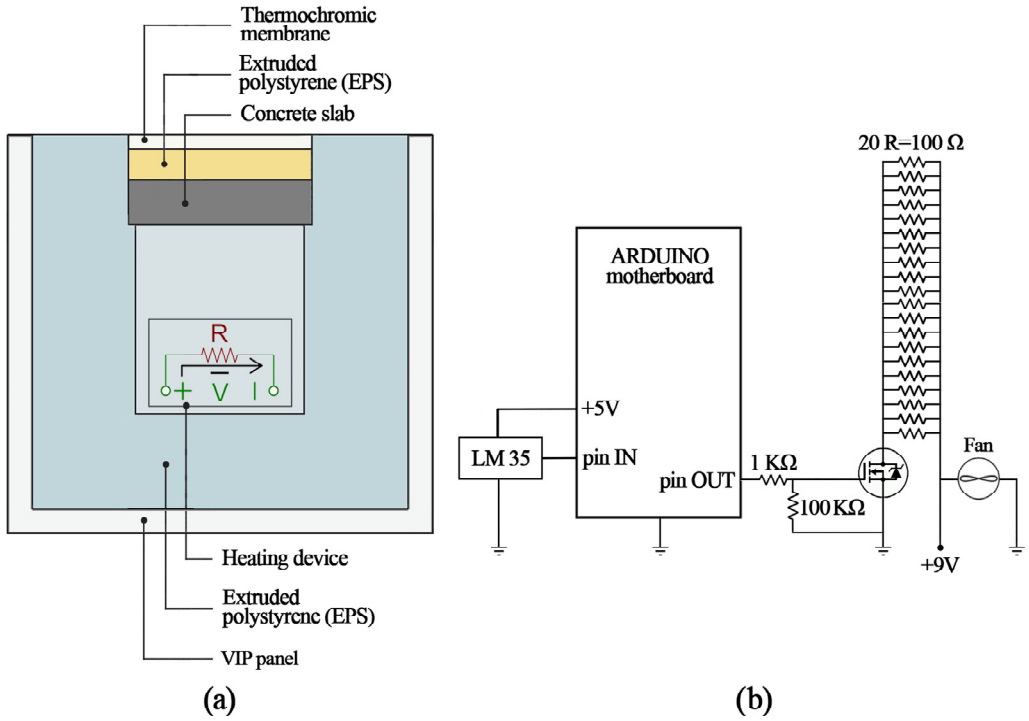

Fig. 4. (a) Experimental setup and (b) sketch of the heater device.

Table 2
Main thermophysical properties, i.e. k (thermal conductivity), c_p (volumetric heat capacity), Y (periodic thermal transmittance), and thickness (d) of the simulated and equivalent experimental stratigraphy considered and of the insulation box.

Simulated stratigraphy (SIMstr)				
Material	k [W m^{-1} K^{-1}]	c_p [MJ m^{-3} K^{-1}]	Y [W m^{-1} K^{-1}]	d [m]
SIMstr	0.94	1.50	0.731	0.300
Equivalent experimental stratigraphy (EQstr)				
Material	k [W m^{-1} K^{-1}]	c_p [MJ m^{-3} K^{-1}]	Y [W m^{-1} K^{-1}]	d [m]
PUR-TC membrane	0.28	0.90	–	0.015
XPS	0.034	1.3	–	0.035
Concrete slab	1.77	1.0	–	0.050
EQstr	0.09	1.14	0.722	0.100
Insulation box (Box)				
Material	k [W m^{-1} K^{-1}]	c_p [MJ m^{-3} K^{-1}]	Y [W m^{-1} K^{-1}]	d [m]
VIP	0.002	⟶0	–	0.015
XPS	0.034	1.3	–	0.100
Box	0.010	0.07	0.083	0.115

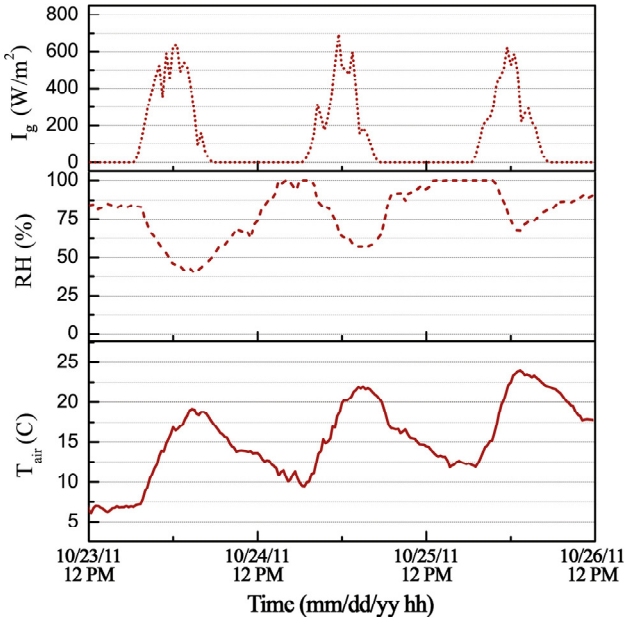

Fig. 5. Imposed environmental cycle reproducing the global radiation (I_g), relative humidity (RH) and air temperature (T_{air}) conditions of the period October 23–26th 2011.

hygrothermal condition of three representative days in the transition period, i.e. October 23–26th 2011 (see Fig. 5). Since the UCM model considers a fixed internal temperature during the overall duration of the simulation, a portable heating device was produced using Arduino and placed within the insulated box to guarantee the selected temperature (25 °C) in the confined air volume. A sketch of the device is represented in Fig. 4b. According to the scheme, the heater only generates heat when the switch on/off system is activated by a temperature trigger (given by a LM35 sensor with an accuracy of 0.5 °C). The heat is produced by Joule effect using twenty 100 Ω resistors connected in parallel. A 9 V fan was also connected to the system in order to ensure homogeneous temperature distribution within the box.

A chilling system would have required a more complex experimental setup; for this reason, the validation procedure was carried out considering three days in October characterized by an average air temperature of about 14.6 °C, and a maximum and minimum temperature of about 24.0 and 6.1 °C, respectively. However, due to the intense contribution from the solar radiation, the maximum sol-air temperature ($T_{Sol-air}$ measured in °C) rose to maximum value of about 28.4 °C, i.e. above the transition threshold for the selected thermochromic pigment and also above the fixed temperature value used for simulating the indoor of the building. $T_{Sol-air}$ can be calculated as a function of the air temperature (T_{air} measured in °C), the absorption coefficient of the surface (α_{rad}), the global radiation (I_g measured in $W \cdot m^{-2}K$) and the external surface resistance (R_{se} measured in $W \cdot m^{-2}\dot{K}^{-1}$) as [54]

$$T_{Sol-air} = T_{air} + \alpha_{rad} I_g R_{se} \quad (5)$$

However, since superficial temperatures above 25 °C are expected to be kept for a short time, the need for internal cooling in the box should be unecessary. To double check this assumption, several PT-100 thermocouples were used to accurately monitor the evolution of the temperature profiles during the test. Globally, 12 PT-100 sensors were used during the experimental campaign:

- 4 within the air domain enclosed in the experimental setup;
- 4 on the top of the equivalent stratigraphy (outdoor surface);
- 4 at the bottom of the equivalent stratigraphy (indoor surface).

3.3. Numerical experiments design

Three different numerical analyses were carried out in this work. First, the effect of the experimentally developed thermochromic roof coating, characterized by a 20 °C transition temperature (TT) was assessed and benchmarked with respect to a traditional dark roof configuration ($\alpha = 0.15$), and a realistic soiled cool roof ($\alpha = 0.55$). At a later stage, the potential effect of an improved membrane capable of tailoring its albedo between the reference limits of the dark ($\alpha = 0.15$) and the cool membrane ($\alpha = 0.55$) was investigated. In this case a thermochromic transition temperature of 30 °C was considered. Finally, the transition temperature (TT) of the thermochromic material was varied between 20 and 40 °C, with a step of 5 °C and the obtained results were compared considering the thermochromic variation range of application (ii).

In-situ observations collected in Princeton, NJ, were used to drive the simulations from May 2011 to April 2012, and diurnal profiles where averaged for each of the simulated months. The considered urban canyon was characterized by an aspect ratio (building height to canyon width) of 0.80 and an impervious area fraction of 0.84. The

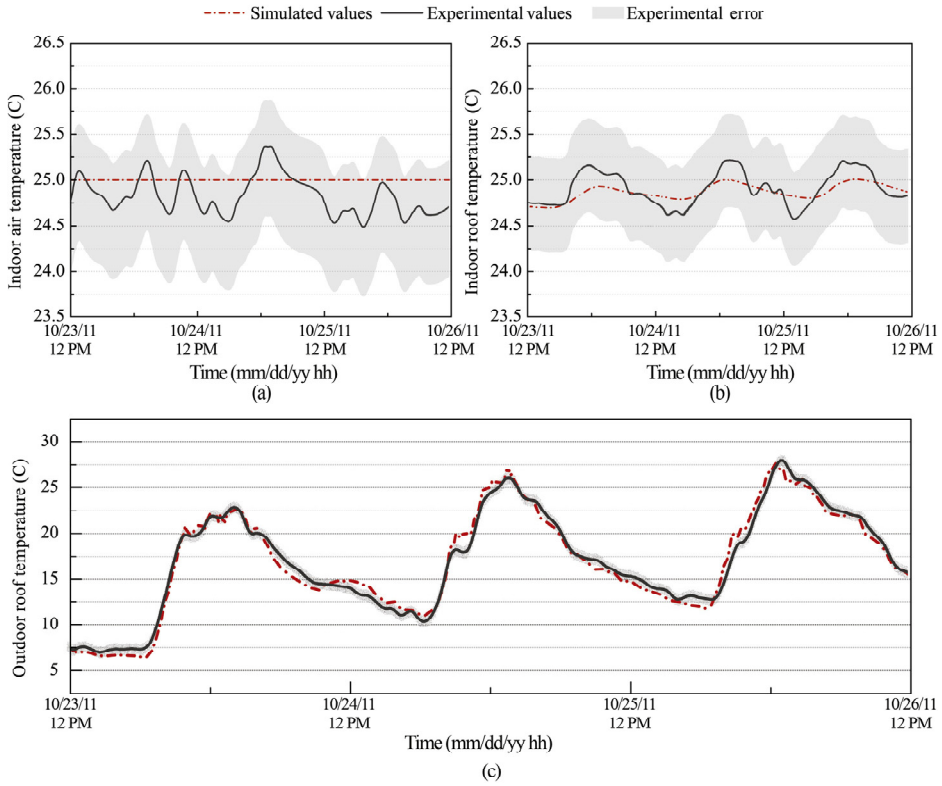

Fig. 6. Comparison between the simulated and the experimental temperature profiles obtained on (a) the indoor air volume, (b) the inner and (c) the outer surface of the roof stratigraphy in the period October 23–26th 2011..

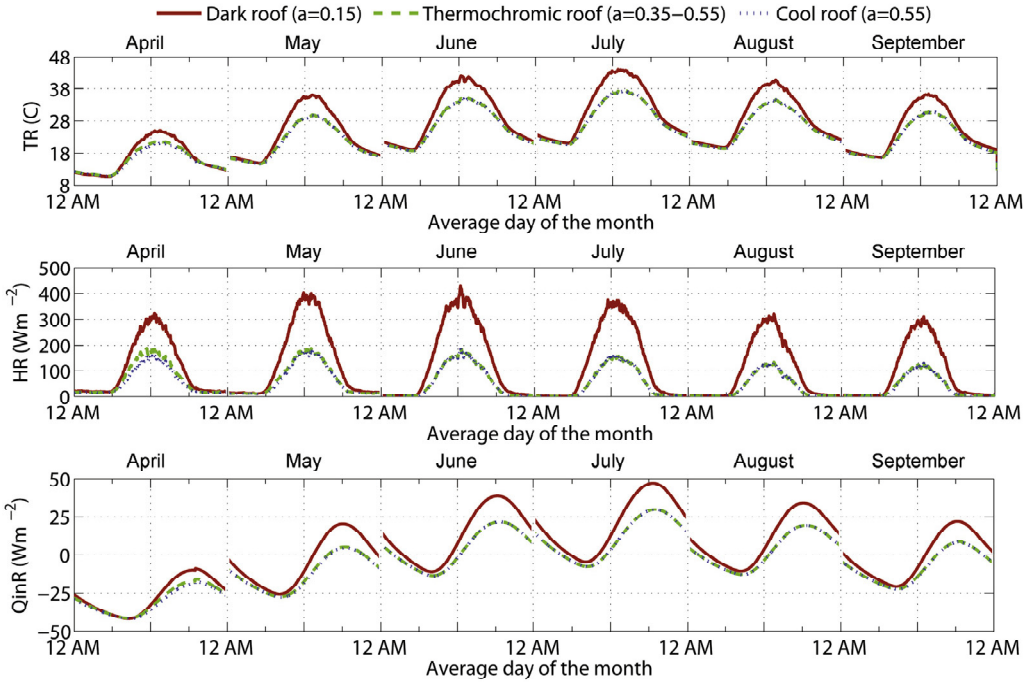

Fig. 7. Dark ($\alpha = 0.15$), thermochromic ($\alpha = 0.35 - 0.55$) and cool ($\alpha = 0.55$) external roof surface temperature (TR), outward sensible heat flux (HR) and inward heat flux (QinR) monthly-averaged diurnal cycles for the six spring and summer months.

town is thus densely urbanized but its spatial extent is limited, which minimizes its impact on the atmospheric variables and makes it suitable for offline UCM applications and testing. The observations are obtained from a dedicated weather station with a 30-min time resolution. Specifically, the model requires the following driving atmospheric variables: air temperature, specific humidity, atmospheric pressure, wind speed, shortwave solar radiation, long-wave solar radiation and precipitation data, which were interpolated from the original weather file to fit the simulation time interval ($dt = 10s$), throughout the simulation.

4. Results and discussions

4.1. Model validation

Fig. 6 shows the results obtained from the thermal monitoring of the equivalent roof stratigraphy during the simulated transition period. As can be seen, each thermal profile obtained from the numerical simulation very well reproduces the specific monitored trend. The indoor air temperature is a model input and the experimental design ensured that the experimental value was always close to the modeled one. As a result, the simulated surface temperature at the internal surface layer of the investigated stratigraphy is also within the experimental error range of the observations. The most challenging temperature for the model to reproduce is the outdoor surface temperature, and while the monitored and simulated trends are not always equal, within the experimental error, the obtained profiles are in very good accordance during the whole monitored period (root mean square error RMSE = 0.8398). Of particular significance here is the fact that the potential model error is much smaller than the diurnal swings in outdoor surface temperature, which is the signal we are mostly interested in. These results indicate that the implemented numerical model can accurately describe the thermo-optical behavior of the investigated thermochromic roof coating.

4.2. Comparison of dark, cool and thermochromic roofs

Results from the comparison among the experimentally developed thermochromic membrane and the dark and cool roof configuration are shown in Figs. 7 and 8 in terms of roof surface temperature (TR), outward sensible heat flux at the outer surface (HR) and heat flux at the inner wall surface into the indoor space (QinR). The dark roof profiles are always associated with the largest fluctuations, while the cool roof always presents the lowest surface temperature and heat fluxes. This cool roof behaviour is good in terms of UHI mitigation potential during the hottest months of the year, where this roof is positively affected by the reduced radiative absorption of incoming solar radiation. While the cool roof impact on building-scale winter-heating energy consumption is not very significant if the building is well insulated [50,55], cool roofs inevitably negate some of the winter-time benefits of the UHI at the city-scale by reducing its intensity [32]. Our results indeed confirm this as illustrated by the reduction in HR in the winter months relative to dark roofs.

The thermochromic roof, on the other hand, shows the interesting capability to dampen the heat gains during summer, while preserving the beneficial behavior of the dark roof both in autumn and winter. As a matter of fact, during these months the roof surface temperature rarely exceeds the thermochromic transition, and consequently a lower albedo is assumed by the roof, which is allowed to absorb a higher amount of energy from the incident solar radiation.

Similar results are also found in the comparison of the advanced thermochromic membrane, capable of varying its solar reflectance value between the lower limit of the dark and the upper limit of the cool roof solution (see Figs. 9 and 10). However, in this case the numerical model shows that by allowing the membrane to dynamically switch between 0.15 and 0.55, the detrimental winter penalty of the cool roof configuration could be completely avoided in the colder months, while in the first application they were just significantly reduced.

The atypical temperature and heat fluxes profiles obtained for the thermochromic roof are a consequence of its dynamic nature that allows it to adjust its ability to reflect the visible incoming radiation as a function of the local surface temperature. Fig. 11 shows the albedo variation profile obtained for the thermochromic roof during representative weeks in May, July, October and January. As can be seen, each time the roof temperature exceeds the thermochromic transition temperature TT, the albedo starts to increase, and finally reaches the cool roof limit value of 0.55. This limit is generally exceeded every day during the hottest months, while in winter this almost never happens. On cloudy days in the spring and autumn, numerous transitions can occur. These results are expected since the thermochromic roof is designed as such, and hence they mainly serve as an additional validation of the implementation. Now we turn our attention to the analysis of the less-obvious performance indicators of thermochromic roofs.

The introduction of the thermochromic roof coating has positive effects in terms of temperature and inward heat flux stabilization, as illustrated in Figs. 12, which shows the standard deviation trends calculated for each monthly-averaged diurnal cycle in spring and summer.

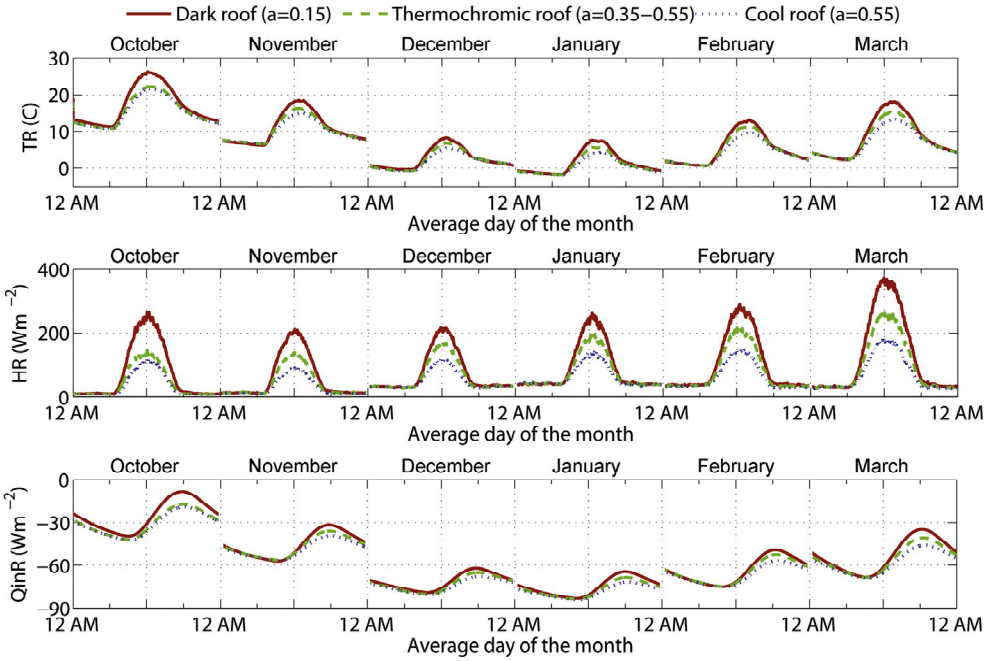

Fig. 8. Dark (α = 0.15), thermochromic (α = 0.35 − 0.55) and cool (α = 0.55) external roof surface temperature (TR), outward sensible heat flux (HR) and inward heat flux (QinR) monthly-averaged diurnal cycles for the six autumn and winter months.

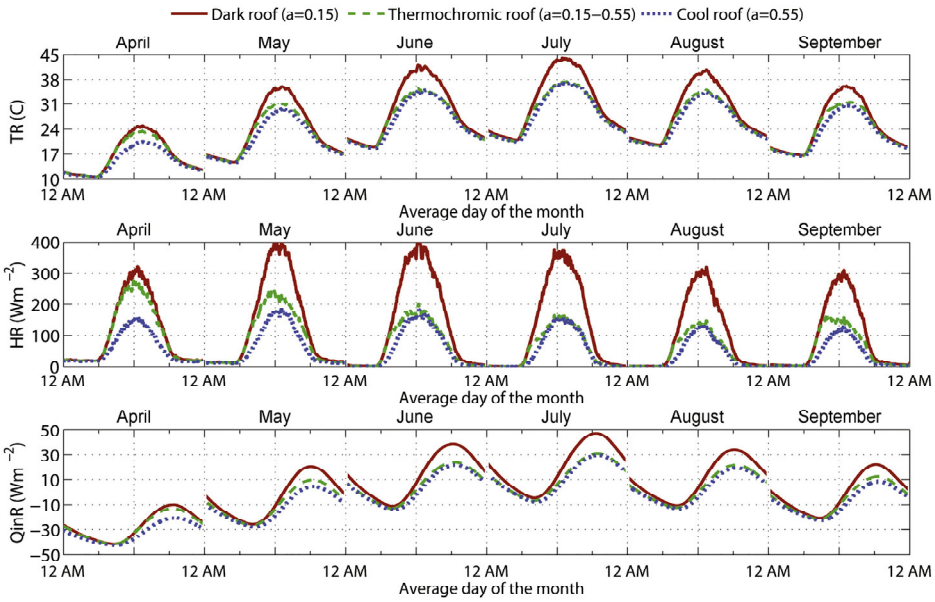

Fig. 9. Dark ($\alpha = 0.15$), thermochromic ($\alpha = 0.15 - 0.55$) and cool ($\alpha = 0.55$) external roof surface temperature (TR), outward sensible heat flux (HR) and inward heat flux (QinR) monthly-averaged diurnal cycles for the six spring and summer months.

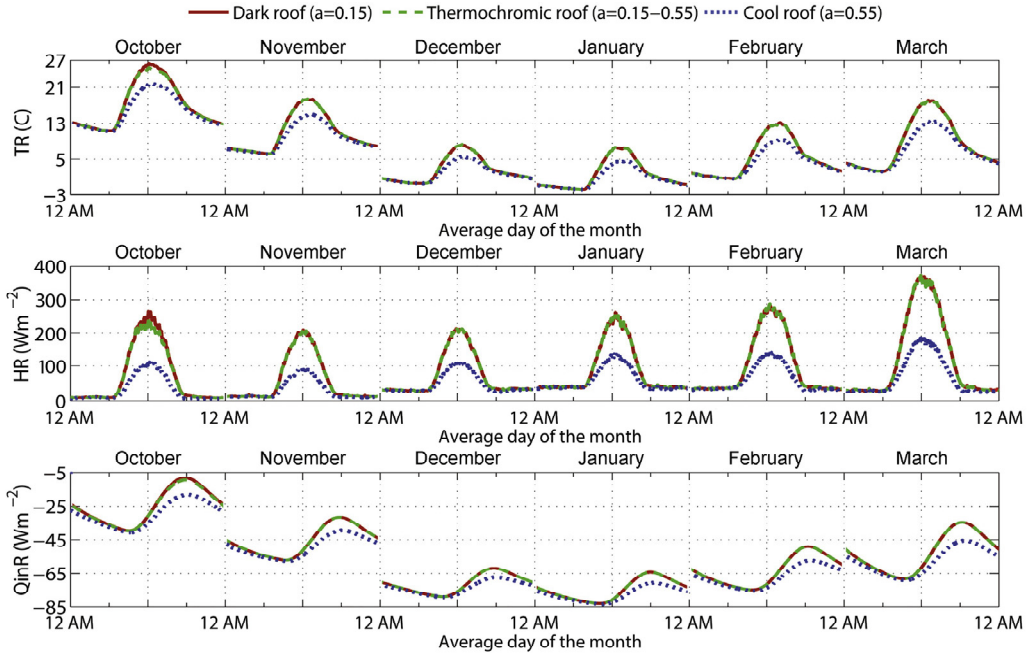

Fig. 10. Dark ($\alpha = 0.15$), thermochromic ($\alpha = 0.15 - 0.55$) and cool ($\alpha = 0.55$) external roof surface temperature (TR), outward sensible heat flux (HR) and inward heat flux (QinR) monthly-averaged diurnal cycles for the six autumn and winter months.

Similar values are also obtained during autumn and winter, but are not reported here due to space constraints. The introduction of the dynamic material, in fact, produces more regular temperature and inward sensible heat flux trends during Spring and Summer, compared to both the dark and the cool configuration. This smooths the cooling energy demand curve and could be an additional positive effect of such an innovative application. In addition, the theory of the adaptive thermal comfort builds on the principle that people can, up to a certain extent, adapt to a variety of indoor conditions, and that they experience these conditions differently depending on their clothing, their activity, their general physical condition and also on the environmental stimuli that they have been experiencing in priori days [56]. All this considered, if the thermochromic coating is capable of maintaining a more stable energy transfer through the building envelope, it is reasonable to think that it would also increase the occupant resilience to the local environment, and indirectly reduce energy consumption in summer.

From an energy point of view, it is possible to compare the amount of energy flowing through the roof of the building of the cool and thermochromic configuration, to the original traditional dark roof. To do this, the cumulative energy loads deriving from the heat exchanged through 1 square meter of roof were calculated assuming that the heating and cooling systems of the building were turned on by the user if the average outdoor air temperature was below or above the base temperature of 18 °C, respectively [57].

Fig. 13 shows that the implementation of a cool roof reduces the amount of energy gained through the building during summer months,

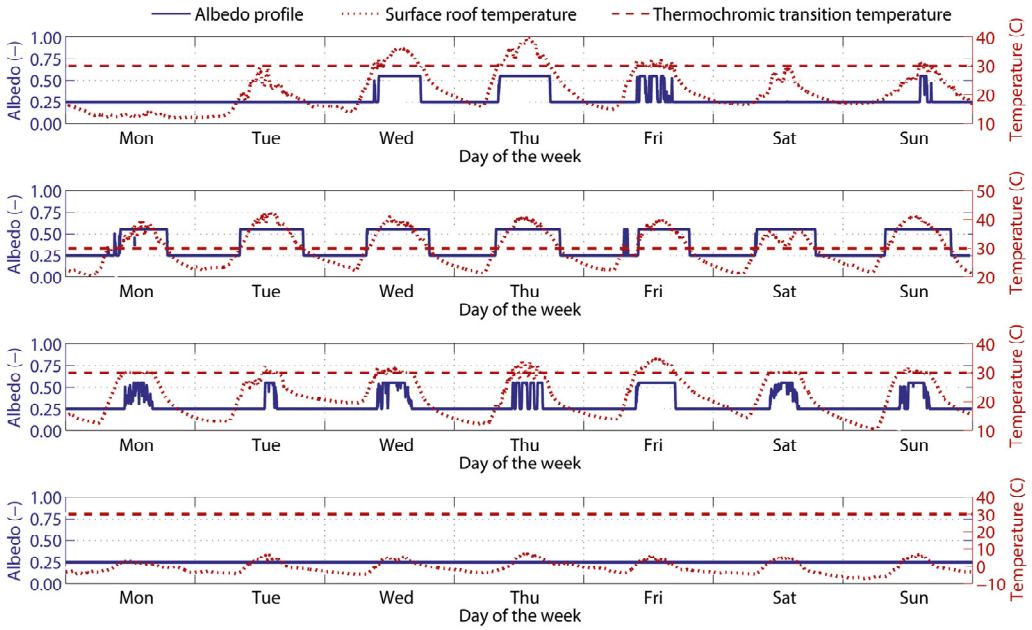

Fig. 11. Albedo profile for a representative week in (from top to bottom) May, July, October and January.

by up to 6.584 kWh m^{-2} in July, compared to the original dark roof, but it is always associated with non negligible energy losses during the colder months. By using the thermochromic coating, on the other hand, the energy gain reduction is only marginally reduced, i.e. to 5.848 kWh m^{-2}, below the dark roof in July. However, the winter penalty of the high albedo configuration is completely canceled in the colder months, i.e. from October to March, and significantly reduced in the transition period, i.e. in April, May and September. Globally, as can be seen in Table 3, the thermochromic configuration reduces the energy loads for cooling during the year by 20.779 kWh m^{-2} (about 6.59% of the cumulative energy load produced by the traditional roof scenario), while the additional loads for heating remain below 0.217%. The cool roof solution, on the other hand, allows to obtain higher savings in summer, i.e. −24.718 kWh m^{-2} compared to the dark configuration, but inevitably suffers from the higher energy losses in the period between September and May, increasing the heating loads by 18.498 kWh m^{-2}, i.e. about 5.87%, relative to the black roof (though this also depends on the assumed roof insulation).

4.3. Comparison among different thermochromic transition temperatures

In this section, the results from the comparison of five thermochromic materials characterized by the same albedo range, i.e. 0.15–0.55, but different transition temperatures, i.e. TT = 20, 25, 30, 35 and 40 °C, are presented. In this case, each considered configuration is associated with a material that is dynamically tuning its albedo in response to the experienced temperature boundary condition. However, by selecting different transition temperatures, it is possible to control

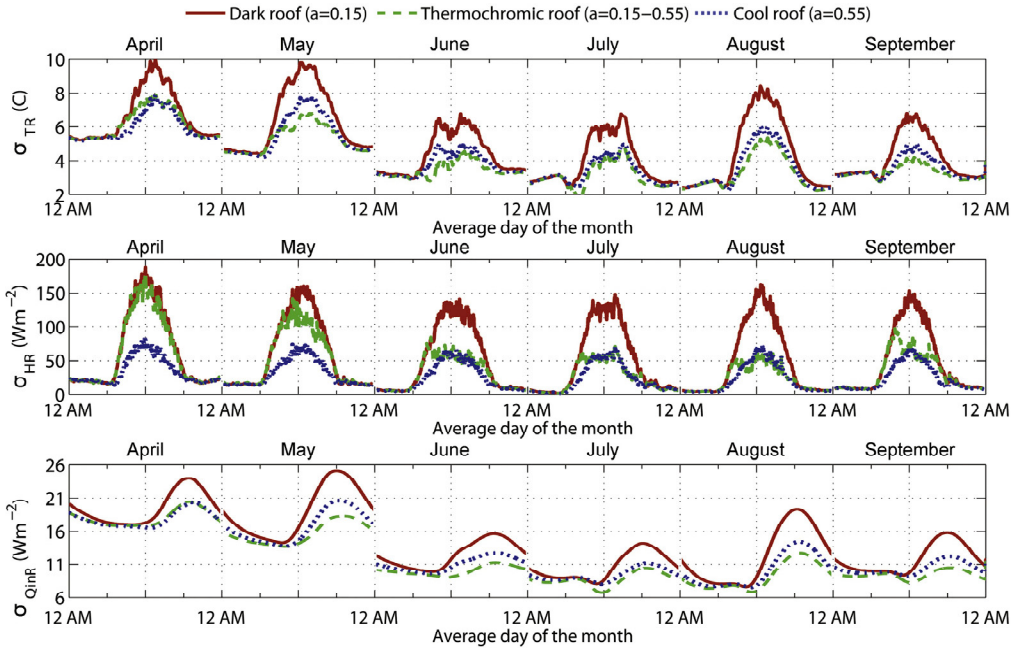

Fig. 12. Dark, thermochromic and cool roof standard deviations of surface temperature (σ_{TR}), outward sensible heat flux (σ_{HR}) and inward heat flux (σ_{QinR}) for the monthly-averaged diurnal cycles of the six spring and summer months.

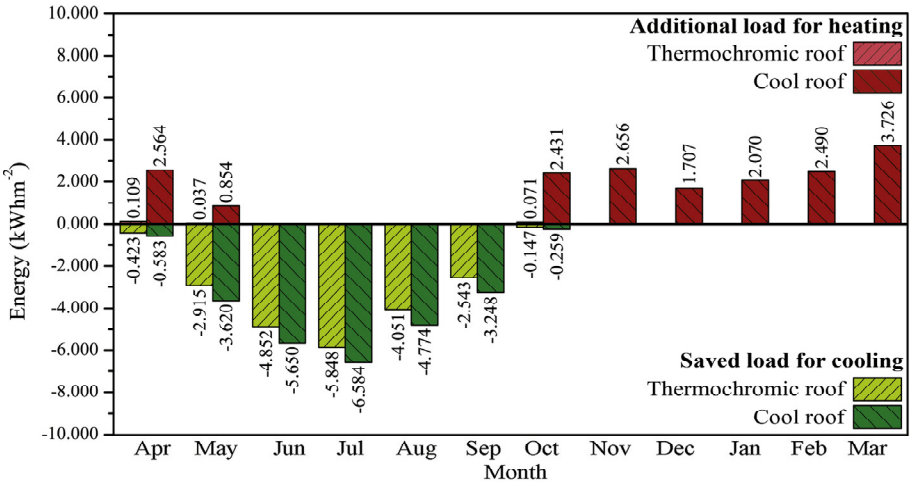

Fig. 13. Difference between the cumulative energy load per meter square of the thermochromic or cool roof, relative to the dark roof, for each simulated month.

Table 3
Cumulative saved energy loads (for cooling) and additional energy loads for (heating) per meter square of thermochromic and cool roof, compared to the common dark roof (the percentage value refers to the sum of the cooling and heating energy loads).

UCM configuration	Saved load for cooling (kWh m^{-2})	(%)	Additional load for heating (kWh m^{-2})	(%)
Thermochromic roof	−20.779	−6.59	+0.217	+0.07
Cool roof	−24.718	−7.84	+18.498	+5.87

the thermochromic transition trigger, and by doing so, drive the material behavior. In particular, by comparing the obtained albedo profiles during two typical weeks of the transition period, i.e. one week in May and one in October (see Fig. 14), it becomes clear that a lower TT, i.e. 20 °C, increases the probability of transitioning to and maintaining a higher albedo, while when the highest TT is chosen, i.e. 40 °C, the thermochromic material will probably maintain its low albedo and high absorptivity to solar radiation, unless extreme temperature values are registered during the day.

Consequently, the obtained temperature and heat flux profiles will show fairly different trends, depending on the selected transition temperature of each configuration (see Figs. 15 and 16). In particular, The most effective transition temperature in terms of UHI mitigation potential seems to be the lowest one, although similar performances are also registered for the 25 and the 30 °C limits. The winter penalty that generally characterizes cool roof applications, on the other hand, does not seem to represent a significant problem even when the 20 °C TT is considered. Additionally, as can be seen in Fig. 17 for the period between October and March, this last configuration seems to be the most effective one in stabilizing the energy budget of the roof during the month, and because of this, it would probably be the most convenient in terms of occupants' adaptive thermal comfort perception. Once again, a similar stabilization effect can also be found during the hotter months

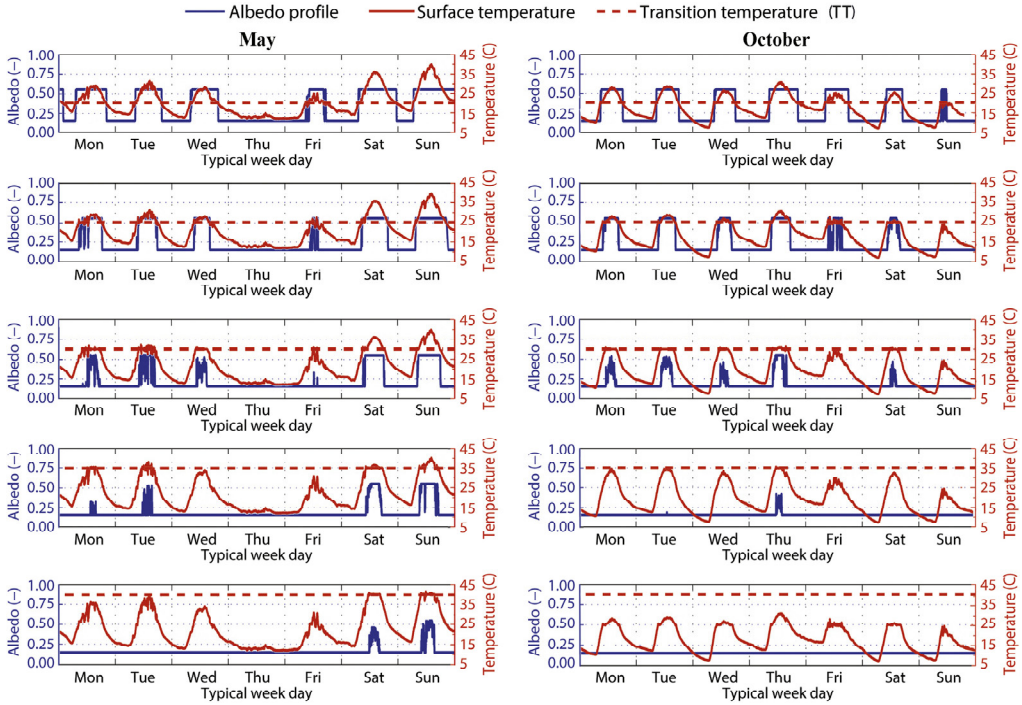

Fig. 14. Albedo profile for two representative weeks in May (left) and in October (right), for the five considered transition temperatures, i.e. from top to bottom TT = 20, 25, 30, 35 and 40 °C.

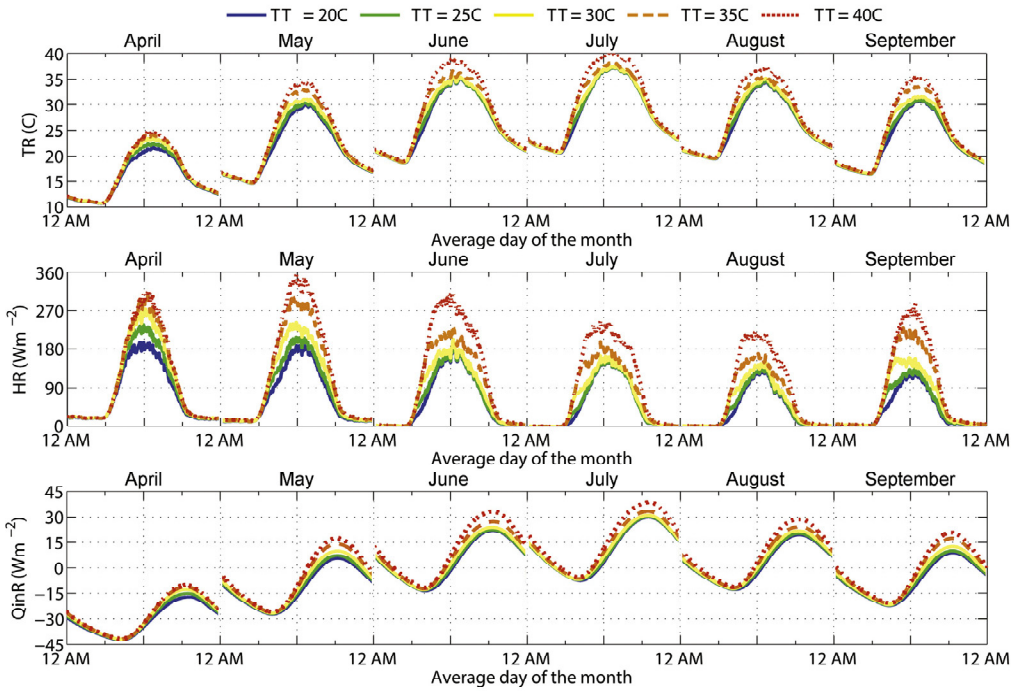

Fig. 15. Roof external surface temperature (TR), outward sensible heat flux (HR) and inward heat flux (QinR) monthly-averaged diurnal cycles of the six spring and summer months, for the five considered transition temperatures, i.e. 20, 25, 30, 35 and 40 °C.

but is not reported here due to space constraints.

However, when dealing with applications based on thermochromic materials, it is also important to preserve the dynamic nature that allows them to adapt to local boundary conditions. Of course, the higher the number of thermochromic transitions undergone by the material, the higher the deterioration of the material itself will be. Therefore, in this work, the amount of thermochromic transitions, intended as triggering of the colouring and de-colouring phase, are also investigated, together with the amount of time in which the thermochromic material behaves as a common cool coating, i.e. albedo of 0.55. Fig. 18 shows the total number of thermochromic activations undergone by the 5 different roof coatings in each of the considered months (remember that the code considers a time step of 10 s), and the percentage of time in which the roof has by an α value of 0.55. The cumulative values are reported in Table 4.

These results show that, even though the UCM configuration with a TT value of 40 °C is associated with the highest number of thermochromic activations during the hottest months and in the whole year

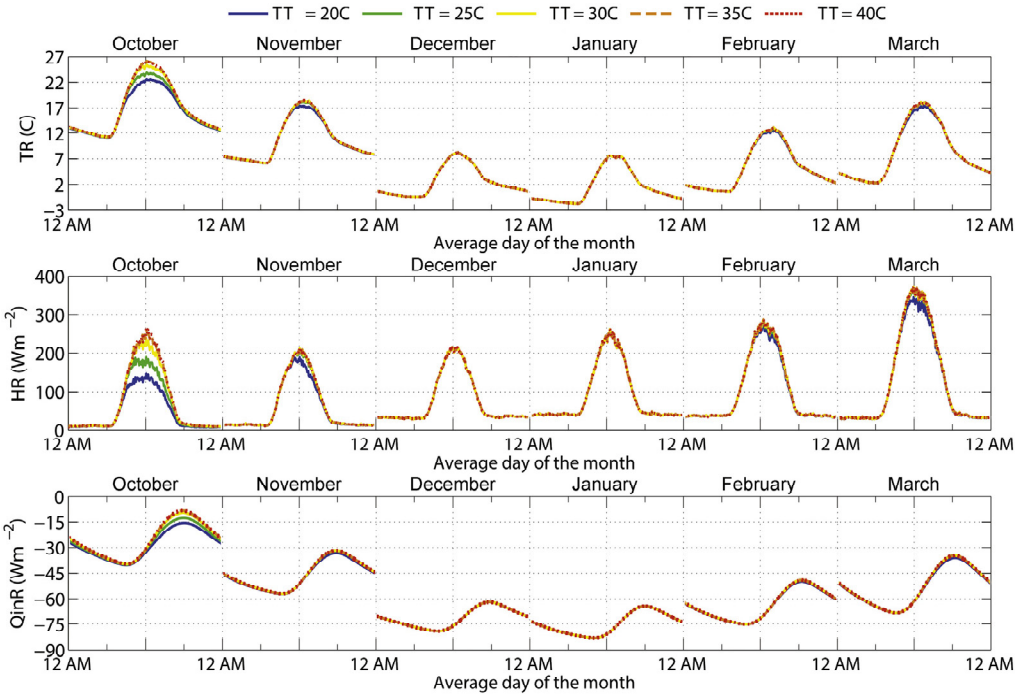

Fig. 16. Roof external surface temperature (TR), outward sensible heat flux (HR) and inward heat flux (QinR) monthly-averaged diurnal cycles of the autumn and winter months, for the five considered transition temperatures, i.e. 20, 25, 30, 35 and 40 °C.

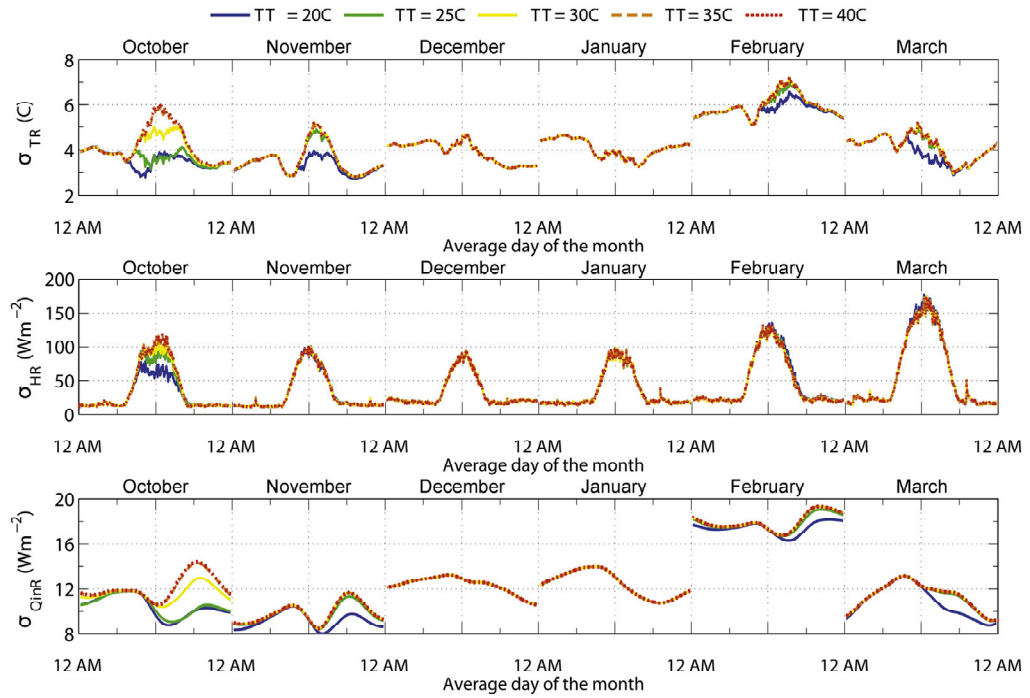

Fig. 17. Standard deviation of external roof surface temperature (TR), outward sensible heat flux (HR) and inward heat flux (QinR) for the monthly-averaged diurnal cycles of the autumn and winter months, for the five considered transition temperatures, i.e. 20, 25, 30, 35 and 40 °C.

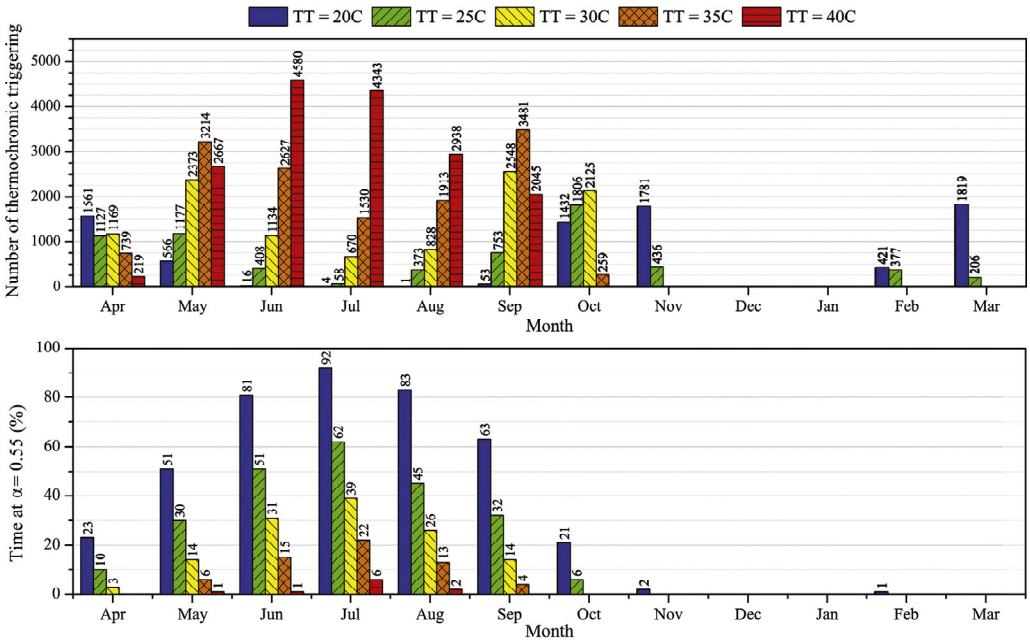

Fig. 18. Cumulative number of thermochromic triggering (top) and percentage of time at $\alpha = 0.55$ (bottom) for the five considered transition temperatures, i.e. 20, 25, 30, 35 and 40 °C in each of the simulated month.

Table 4
Cumulative number of thermochromic transitions and percentage of time spent at $\alpha = 0.55$ for the five considered transition temperatures, i.e. 20, 25, 30, 35 and 40 °C.

UCM configuration	TT = 20 °C	TT = 25 °C	TT = 30 °C	TT = 35 °C	TT = 40 °C
Number of transitions	7654	6721	10847	13763	16792
Time at $\alpha = 0.55$ (%)	35.09	19.82	10.65	4.92	0.87

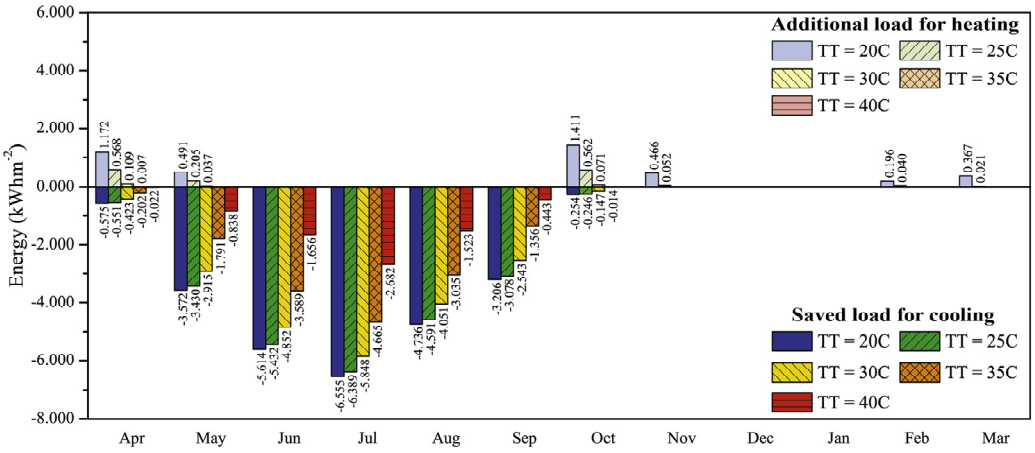

Fig. 19. Difference between the cumulative energy amount per meter square of dark roof and the five thermochromic configurations, per each simulated month.

(16792), it almost never reaches the highest albedo value during the whole year (only 0.87% of the global time). The scenarios investigating the potential of the 30 and 35 °C transition limit, on the other hand, experience most of the thermochromic transitions between May and September, a period in which they can also maintain the highest α value for an acceptable period of time, i.e. between 14 and 39% and 4 and 22% of the time, respectively.

Finally, the remaining configurations, i.e. 20 and 25 °C, are characterized by fairly lower cumulative number of thermochromic transitions, but because of the reduced temperature limit, they experience these kind of transitions also during colder months such as February and March. However, during summer, this kind of roof coatings maintains its surface temperature above the selected threshold, and because of this, spends most of the time behaving as a cool material. It is noteworthy that the lowest number of thermochromic transition is not associated to the 20 °C configuration, but to the one with the TT equal to 25 °C. This is due to the fact that this thermochromic scenario experiences a lower number of activations during the autumn and the winter season.

Finally, by comparing the amount of energy flowing indoors through the five considered thermochromic roofs and the reference dark configuration, it is possible to investigate the energy benefit of the different thermochromic applications. In particular, Fig. 19 shows that although lower transition temperatures allow to optimize the energy behavior of the building in summer, they also increase the amount of energy losses in the autumn and the spring season, when, for example, 4.103 and 1.447 kWh m^{-2} of additional heating loads are generated using a transition temperature of 20 and 25 °C, respectively. As a matter of fact, and as shown in Table 5, lower TT values increase the winter penalty of the thermochromic roof by values as high as 4.103 kWh m^{-2}, i.e. 1.3% with respect to the final energy loads of the traditional dark configuration are reached if a transition temperature of 20 °C is considered. Consequently, it can be stated that, from an energy point of view, the most promising TT value for the selected boundary conditions and roof insulation is 25 °C.

Table 5
Cumulative saved energy loads (for cooling) and additional energy loads for (heating) per meter square of the different thermochromic roofs, i.e. with a transition temperature of 20, 25, 30, 35 and 40 °C, compared to the common dark roof.

Transition temperature	Saved load for cooling (kWh m^{-2})	(%)	Additional load for heating (kWh m^{-2})	(%)
20 °C	−24.513	−7.8	4.103	1.30
25 °C	−23.716	−7.5	1.447	0.46
30 °C	−20.779	−6.6	0.217	0.07
35 °C	−14.653	−4.6	0.008	0.00
40 °C	−0.046	−2.3	0.000	0.00

5. Concluding remarks

In this work, a numerical model of a thermochromic roof at the interbuilding scale was developed and validated against experimental data. Furthermore, the year-long UHI modulation potential of an advanced roofing solution, capable of dynamically adapting its albedo in the range 0.35–0.55 and 0.15–0.55, was investigated and benchmarked against more common solutions such as a classic dark roof (α = 0.15) and a high-performance soiled cool roof (α = 0.55). Finally, the effect of different thermochromic transition temperatures, i.e. 20, 25, 30, 35 and 40 °C, was assessed with the aim of investigating an optimized application in terms of summertime UHI mitigation potential, building energy consumption for heating and cooling purposes, and weathering of the material. Each of the considered roof configuration was analyzed using year-long simulations in order to evaluate its performance under varying climatic conditions.

Results confirm the beneficial impact of the thermochromic roofs attributed to their ability to dynamically change their albedo to reflect the incoming solar radiation in response to the roof surface temperature. Despite some lag in the transition that was accounted for in the model, when the roof surface is characterized by temperatures below the transition threshold, the thermochromic configuration behaved predominantly as a classic dark roof, allowing the overall urban surface to absorb heat in the form of solar heat gains. This reduces the winter penalty of the high performance cool roof and reproduces the temperature and heat flux profiles of the more convenient dark roof configuration during cooler periods. As a result, the yearly energy balance of the innovative dynamic roof configuration globally enables a 6.59% cooling load reduction per meter square of roof compared to the 7.84% decrease obtained by using a more common cool application. However, in the colder months, when the reduction of the passive solar heating phenomenon severely affects the cool roof performance, generating a 5.87% increase in the thermal loads due to the heat transfer through the roof, the dynamic response of the thermochromic finishing allows to drastically reduce to 0.07% the additional heating loads transmitted through the roof).

Results from the year-long simulations also demonstrated an additional positive effect of the thermochromic roof dynamic nature, that is, its ability to stabilize heat flux and temperature gradients through the building envelope during the year. Consequently, the introduction of this innovative finishing could produce a non-negligible and convenient effect in terms of occupants' adaptive thermal comfort perception, thus producing an additional UHI mitigation effect at the city scale.

Regarding the comparison among several thermochromic transition

temperatures, it was found that thresholds above 30 °C highly reduce the UHI mitigation potential of the thermochromic material, since it rarely behaves as a cool coating in roof applications at the selected latitude. The most promising transition temperature in terms of material durability is that of 25 °C, since it reduces the number of thermochromic transitions experienced by the selected coating while keeping the cool roof behavior for long periods of time. However, from an energy point of view, the most promising final energy balance is obtained using the transition temperature of 30 °C. One should bear in mind however that the benefits of dynamic changes in albedo on cooling and heating loads would decrease with increasing insulation, though the benefits for outdoor climates and comfort remains unchanged. These results naturally apply to climates similar to that of Princeton, NJ, where the forcing data were available, but the general point is that different transition temperatures have an impact on the roof thermal energy performance and this property can be potentially tailored for local climates and for specific roofs.

In conclusion, using adaptive materials such as thermochromic solutions in building roofs can indeed be considered as a promising solution to mitigate the increase of air temperatures in the urban environment during summer overheated conditions, while maintaining the positive absorption of solar radiation in winter. All this considered, future research should assess the long term stability of this kind of dynamic materials and evaluate the feasibility of real scale applications in the urban environment.

Acknowledgment

This work was carried out thanks to the support of H2CU, the Honors Center of Italian Universities for International Scientific Cooperation. The first author is supported by Ministry funding and university funding of the PhD school in Energy and Sustainable Development. The authors from Princeton University are supported by the US National Science Foundation under Grant No. ICER 1664091 and under the UWIN Sustainability Research Network Cooperative Agreement 1444758.

References

[1] Yin C, Yuan M, Lu Y, Huang Y, Liu Y. Effects of urban form on the urban heat island effect based on spatial regression model. Sci Total Environ 2018;634:696–704. https://doi.org/10.1016/J.SCITOTENV.2018.03.350. URL <https://www.sciencedirect.com/science/article/pii/S0048969718311100?via%3Dihub>.

[2] Kolokotroni M, Giridharan R. Urban heat island intensity in London: an investigation of the impact of physical characteristics on changes in outdoor air temperature during summer. Sol Energy 2008;82(11):986–98. https://doi.org/10.1016/J.SOLENER.2008.05.004. URL <https://www.sciencedirect.com/science/article/pii/S0038092X08001084>.

[3] Xu X, González JE, Shen S, Miao S, Dou J. Impacts of urbanization and air pollution on building energy demands — Beijing case study. Appl Energy 2018;225:98–109. https://doi.org/10.1016/J.APENERGY.2018.04.120. URL <https://www.sciencedirect.com/science/article/pii/S0306261918306883?via%3Dihub#>.

[4] Solecki W, Marcotullio PJ. Climate change and urban biodiversity vulnerability. In: Elmqvist T, Fragkias M, Goodness J, Guneralp B, Marcotullio PJ, McDonald RI, editors. Urbanization, biodiversity and ecosystem services: challenges and opportunities: a global assessment. Netherlands: Springer; 2013. p. 485–504.

[5] Lowe SA. An energy and mortality impact assessment of the urban heat island in the US. Environ Impact Assess Rev 2016;56:139–44. https://doi.org/10.1016/J.EIAR.2015.10.004. URL <https://www.sciencedirect.com/science/article/pii/S0195925515001043>.

[6] Sarrat C, Lemonsu A, Masson V, Guedalia D. Impact of urban heat island on regional atmospheric pollution. Atmos Environ 2006;40(10):1743–58. https://doi.org/10.1016/J.ATMOSENV.2005.11.037. URL <https://www.sciencedirect.com/science/article/pii/S1352231005010885>.

[7] Founda D, Santamouris M. Synergies between Urban Heat Island and Heat Waves in Athens (Greece), during an extremely hot summer (2012). Sci Rep 2017;7(1):1–11. https://doi.org/10.1038/s41598-017-11407-6.

[8] Heaviside C, Vardoulakis S, Cai XM. Attribution of mortality to the urban heat island during heatwaves in the West Midlands, UK. Environ Health: A Glob Access Sci Sour 2016;15(Suppl 1). https://doi.org/10.1186/s12940-016-0100-9.

[9] Li D, Bou-Zeid E. Synergistic interactions between urban heat islands and heat waves: the impact in cities is larger than the sum of its parts. J Appl Meteorol Climatol 2013;52(9):2051–64. https://doi.org/10.1175/JAMC-D-13-02.1.

[10] Zhao L, Oppenheimer M, Zhu Q, Baldwin JW, Ebi KL, Bou-Zeid E, et al. Interactions between urban heat islands and heat waves. Environ Res Lett 2018;13(3):034003. https://doi.org/10.1088/1748-9326/aa9f73. URL <http://stacks.iop.org/1748-9326/13/i=3/a=034003?key=crossref.11cceae00694f6275f6a1d9cb94fc02d>.

[11] Santamouris M. Cooling the cities – a review of reflective and green roof mitigation technologies to fight heat island and improve comfort in urban environments. Sol Energy 2014;103:682–703. https://doi.org/10.1016/J.SOLENER.2012.07.003. URL <https://www.sciencedirect.com/science/article/pii/S0038092X12002447>.

[12] Ihara T, Kikegawa Y, Asahi K, Genchi Y, Kondo H. Changes in year-round air temperature and annual energy consumption in office building areas by urban heat-island countermeasures and energy-saving measures. Appl Energy 2008;85(1):12–25. https://doi.org/10.1016/J.APENERGY.2007.06.012. URL <https://www.sciencedirect.com/science/article/pii/S0306261907000888?via%3Dihub>.

[13] Kikegawa Y, Genchi Y, Kondo H, Hanaki K. Impacts of city-block-scale countermeasures against urban heat-island phenomena upon a building's energy-consumption for air-conditioning. Appl Energy 2006;83(6):649–68. https://doi.org/10.1016/j.apenergy.2005.06.001.

[14] Borbora J, Das AK. Summertime Urban Heat Island study for Guwahati City, India. Sustain Cities Soci 2014;11:61–6. https://doi.org/10.1016/j.scs.2013.12.001.

[15] O'Malley C, Piroozfar P, Farr ER, Pomponi F. Urban Heat Island (UHI) mitigating strategies: a case-based comparative analysis. Sustain Cities Soc 2015;19:222–35. https://doi.org/10.1016/J.SCS.2015.05.009. URL <https://www.sciencedirect.com/science/article/pii/S2210670715000657>.

[16] Li D, Bou-Zeid E, Oppenheimer M. The effectiveness of cool and green roofs as urban heat island mitigation strategies. Environ Res Lett 2014;9(5). https://doi.org/10.1088/1748-9326/9/5/055002.

[17] Sohaili J, Yan LK, Muniyandi SK, Mohamad SS. Urban heat island mitigation using green roof approach. J Teknol 2018;80(3):61–8. https://doi.org/10.11113/jt.v75.5239.

[18] Moghbel M, Erfanian Salim R. Environmental benefits of green roofs on microclimate of Tehran with specific focus on air temperature, humidity and CO_2 content. Urban Climate 2017;20:46–58. https://doi.org/10.1016/j.uclim.2017.02.012.

[19] Chun B, Guldmann JM. Impact of greening on the urban heat island: seasonal variations and mitigation strategies. Comput Environ Urban Syst 2018;71(September):165–76. https://doi.org/10.1016/j.compenvurbsys.2018.05.006.

[20] Sun T, Bou-Zeid E, Ni GH. To irrigate or not to irrigate: analysis of green roof performance via a vertically-resolved hygrothermal model. Build Environ 2014;73(0):127–37. https://doi.org/10.1016/j.buildenv.2013.12.004. URL <http://www.sciencedirect.com/science/article/pii/S0360132313003508papers3://publication/uuid/E972339B-485B-4396-AB1A-0277FFC7525A>.

[21] Azeñas V, Cuxart J, Picos R, Medrano H, Simó G, López-Grifol A, et al. Thermal regulation capacity of a green roof system in the mediterranean region: The effects of vegetation and irrigation level. Energy Build 2018;164:226–38. https://doi.org/10.1016/j.enbuild.2018.01.010.

[22] Yang J, Wang Z-H. Planning for a sustainable desert city: the potential water buffering capacity of urban green infrastructure. Landscape Urban Plan 2017;167:339–47. https://doi.org/10.1016/J.LANDURBPLAN.2017.07.014. URL <https://www.sciencedirect.com/science/article/pii/S0169204617301767>.

[23] Pisello AL. State of the art on the development of cool coatings for buildings and cities. Sol Energy 2017;144:660–80.

[24] Synnefa A, Santamouris M, Apostolakis K. On the development, optical properties and thermal performance of cool colored coatings for the urban environment. Sol Energy 2007;81(4):488–97. https://doi.org/10.1016/J.SOLENER.2006.08.005. URL <https://www.sciencedirect.com/science/article/pii/S0038092X06002039>.

[25] Mangiarotti A, Paoletti I, Morello E. A model for programming design interventions aimed at reducing thermal discomfort in urban open spaces: a case study on the Politecnico di Milano Campus. J Green Build 2008;3(4):119–29.

[26] Levinson R, Akbari H, Reilly JC. Cooler tile-roofed buildings with near-infrared-reflective non-white coatings. Build Environ 2007;42(7):2591–605. https://doi.org/10.1016/J.BUILDENV.2006.06.005. URL <https://www.sciencedirect.com/science/article/pii/S036013230600151X>.

[27] Pisello A, Fortunati E, Mattioli S, Cabeza L, Barreneche C, Kenny J, et al. Innovative cool roofing membrane with integrated phase change materials: experimental characterization of morphological, thermal and optic-energy behavior. Energy Build 2016;112:40–8. https://doi.org/10.1016/J.ENBUILD.2015.11.061. URL <https://www.sciencedirect.com/science/article/pii/S0378778815304254>.

[28] Pisello AL, Fortunati E, Fabiani C, Mattioli S, Dominici F, Torre L, et al. PCM for improving polyurethane-based cool roof membranes durability. Sol Energy Mater Sol Cells 2017;160:34–42. https://doi.org/10.1016/J.SOLMAT.2016.09.036. URL <https://www.sciencedirect.com/science/article/pii/S0927024816303786?via%3Dihub>.

[29] Hosseini M, Akbari H. Heating energy penalties of cool roofs: the effect of snow accumulation on roofs. Adv Build Energy Res 2014;8(1):1–13. https://doi.org/10.1080/17512549.2014.890541.

[30] Pisello AL, Castaldo VL, Fabiani C, Cotana F. Investigation on the effect of innovative cool tiles on local indoor thermal conditions: finite element modeling and continuous monitoring. Build Environ 2016;97:55–68. https://doi.org/10.1016/j.buildenv.2015.11.038.

[31] Yang J, Wang Z-H, Kaloush KE. Environmental impacts of reflective materials: is high albedo a 'silver bullet' for mitigating urban heat island? Renew Sustain Energy Rev 2015;47:830–43. https://doi.org/10.1016/J.RSER.2015.03.092. URL <https://www.sciencedirect.com/science/article/pii/S1364032115002452>.

[32] Yang J, Bou-Zeid E. Should cities embrace their heat islands as shields from extreme cold? J Appl Meteorol Climatol 2018. https://doi.org/10.1175/2010JCLI3851.1.
[33] Ma Y, Zhu B, Wu K. Preparation and solar reflectance spectra of chameleon-type building coatings. Sol Energy 2001;70(5):417–22. https://doi.org/10.1016/S0038-092X(00)00160-2. URL <https://www.sciencedirect.com/science/article/pii/S0038092X00001602>.
[34] Panák O, Držková M, Kaplanová M. Insight into the evaluation of colour changes of leuco dye based thermochromic systems as a function of temperature. Dyes Pigm 2015;120:279–87. https://doi.org/10.1016/j.dyepig.2015.04.022.
[35] Geng X, Li W, Wang Y, Lu J, Wang J, Wang N, et al. Reversible thermochromic microencapsulated phase change materials for thermal energy storage application in thermal protective clothing. Appl Energy 2018;217:281–94. https://doi.org/10.1016/J.APENERGY.2018.02.150. URL <https://www.sciencedirect.com/science/article/pii/S0306261918302800?via%3Dihub>.
[36] Garshasbi S, Santamouris M. Using advanced thermochromic technologies in the built environment: Recent development and potential to decrease the energy consumption and fight urban overheating. Sol Energy Mater Sol Cells 2019;191:21–32. https://doi.org/10.1016/j.solmat.2018.10.023.
[37] Pulit-Prociak J, Banach M. Silver nanoparticles-a material of the future…? Open Chem 2016;14:76–91. https://doi.org/10.1515/chem-2016-0005. URL <https://www.degruyter.com/downloadpdf/j/chem.2016.14.issue-1/chem-2016-0005/chem-2016-0005.pdf>.
[38] Shang L, Gu Z, Zhao Y. Structural color materials in evolution. Mater Today 2016;19(8):420–1. https://doi.org/10.1016/j.mattod.2016.03.004.
[39] Seeboth A, Klukowska A. Thermochromic polymer materials. Chin J Polym Sci 2007;25(2):123–35. https://doi.org/10.1142/S0256767907001923. URL <http://www.worldscientific.com/doi/abs/10.1142/S0256767907001923>.
[40] Sabnis RW. Handbook of acid-base indicators. Handbook Acid-Base Indicators 2007:1–416. https://doi.org/10.1201/9780849382192.
[41] Karlessi T, Santamouris M. Improving the performance of thermochromic coatings with the use of UV and optical filters tested under accelerated aging conditions. Int J Low-Carbon Technol 2015;10(1):45–61. https://doi.org/10.1093/ijlct/ctt027.
[42] Zheng S, Xu Y, Shen Q, Yang H. Preparation of thermochromic coatings and their energy saving analysis. Sol Energy 2015;112:263–71. https://doi.org/10.1016/j.solener.2014.09.049.
[43] Karlessi T, Santamouris M, Apostolakis K, Synnefa A, Livada I. Development and testing of thermochromic coatings for buildings and urban structures. Sol Energy 2009;83(4):538–51. https://doi.org/10.1016/j.solener.2008.10.005.
[44] Li D, Bou-Zeid E. Quality and sensitivity of high-resolution numerical simulation of urban heat islands. Environ Res Lett 2014;9(5). https://doi.org/10.1088/1748-9326/9/5/055001.
[45] Wang Z-H, Bou-Zeid E, Smith JA. A coupled energy transport and hydrological model for urban canopies evaluated using a wireless sensor network. Quart J Roy Meteorol Soc 2013;139(675):1643–57. https://doi.org/10.1002/qj.2032.
[46] Ramamurthy P, Bou-Zeid E, Smith JA, Wang Z, Baeck ML, Saliendra NZ, et al. Influence of subfacet heterogeneity and material properties on the urban surface energy budget. J Appl Meteorol Climatol 2014;53(9):2114–29. https://doi.org/10.1175/JAMC-D-13-0286.1.
[47] Yang J, Wang Z-H, Kaloush KE, Dylla H. Effect of pavement thermal properties on mitigating urban heat islands: a multi-scale modeling case study in Phoenix. Build Environ 2016;108:110–21. https://doi.org/10.1016/J.BUILDENV.2016.08.021. URL <https://www.sciencedirect.com/science/article/pii/S036013231630316X>.
[48] ASTM International, ASTM E903 - 12: Standard Test Method for Solar Absorptance, Reflectance, and Transmittance of Materials Using Integrating Spheres, Tech. rep., ASTM International; 2012.
[49] ASTM-International, Standard Tables for Reference Solar Spectral Irradiances: Direct Normal and Hemispherical on 37° Tilted Surface, Tech. rep., ASTM International; 2013. arXiv:arXiv: 1011.1669v3, doi: https://doi.org/10.1520/G0173-03R12.2. URL < http://enterprise.astm.org/SUBSCRIPTION/filtrexx40.cgi?+REDLINE_PAGES/G173.htm > .
[50] Ramamurthy P, Sun T, Rule K, Bou-Zeid E. The joint influence of albedo and insulation on roof performance: a modeling study. Energy Build 2015;102. https://doi.org/10.1016/j.enbuild.2015.06.005.
[51] Yang J, Wang ZH, Chen F, Miao S, Tewari M, Voogt JA, et al. Enhancing hydrologic modelling in the coupled weather research and forecasting–urban modelling system. Bound-Layer Meteorol 2015;155(1):87–109. https://doi.org/10.1007/s10546-014-9991-6.
[52] Ryu YH, Bou-Zeid E, Wang ZH, Smith JA. Realistic representation of trees in an urban canopy model. Bound-Layer Meteorol 2016;159(2):193–220. https://doi.org/10.1007/s10546-015-0120-y.
[53] ISO, ISO 13786 Thermal performance of building components, Tech. rep., International Organization for Standardization; 1999.
[54] Sá AV, Azenha M, De Sousa H, Samagaio A. Thermal enhancement of plastering mortars with phase change materials: experimental and numerical approach. Energy Build 2012;49:16–27. https://doi.org/10.1016/j.enbuild.2012.02.031.
[55] Ramamurthy P, Sun T, Rule K, Bou-Zeid E. The joint influence of albedo and insulation on roof performance: an observational study. Energy Build 2015;93. https://doi.org/10.1016/j.enbuild.2015.02.040.
[56] European Committee for Standardization, UNI EN 15251:2008 - Indoor environmental input parameters for design and assessment of energy performance of buildings addressing indoor quality air quality, thermal environment, lighting and acoustics. Tech. rep., European Committee for Standardization; 2008.
[57] National Oceanic and Atmospheric Administration (NOAA), National Weather Service, Glossary; 2014. URL < http://www.nws.noaa.gov/glossary/index.php?letter=h > .